ASSESSING THE ANISOTROPIC FEATURES OF LATE REVERBERATION IN A VARIABLE-ACOUSTICS HALL

Alice Pain, Benoit Alary, Stefan Bilbao, Olivier Warusfel

Sorbonne Université, STMS, Ircam, CNRS, Ministère de la Culture, Paris, France

This paper is a revised version of the authors' submitted manuscript that was peer-reviewed by at least two anonymous reviewers.

Abstract

Late reverberation has long been assumed isotropic, i.e., showing a uniform distribution of energy over all angles of incidence. However, recent works leveraging Spherical Microphone Array (SMA) measurements and the associated spatial analysis tools have shown that the isotropy assumption is never perfectly realized. The extent and spatial characteristics of this phenomenon, and its dependence on room geometry, boundary conditions, and transducer positions, require further analysis. This work presents the results of a series of measurements conducted using the em64 Eigenmike (supporting 6th-order Ambisonic encoding), in the Espace de Projection at Ircam, a shoebox-shaped variable-acoustics hall. Spatio-temporal analysis of these measurements reveals a concentration of energy in horizontal axial and tangential modes, influenced by the room geometry. The absorptive boundary conditions induce a noticeably higher anisotropy than the reflective and diffusive conditions. Furthermore, in the case of directive sources, the source orientation has a strong influence on the spatial patterns of anisotropy.

Keywords: *reverberation, anisotropy, spherical microphone array, ambisonics*

1. Introduction

After a sufficient time following a Dirac impulse, room reflections are no longer perceived individually, and the sound field may be described statistically as a combination of infinitely many plane waves with mutually uncorrelated phases. In ideally diffuse conditions, the resulting sound field is homogeneous, i.e., with a uniform distribution of energy over the space, and isotropic, i.e., with a uniform distribution of the angles of incidence at any point in the space [1], [2], [3].

However, perfect isotropy is never fully realized in real enclosures. Anisotropy has been observed in various spaces, ranging from theaters, churches, and opera halls [4], [5] to reverberant chambers [6], [7]. Adding an absorptive sample in a reverberant chamber has been shown to increase anisotropy by introducing non-uniform absorption [7]. The room geometry is expected to influence isotropy, as rectangular enclosures have multiple modes with varying decay rates [8]. Both modal theory [8] and the image source method [9] predict a strong angular dependence of energy decay rates, with axial and tangential modes decaying slower than oblique modes. This is caused by the lack of ergodicity of rectangular enclosures with purely specular reflections [1], [10].

The Espace de Projection (Espro) at Ircam (Fig. 1) is a concert hall with variable acoustics and a near-shoebox shape, making it an interesting study case for room acoustics. The room has dimensions $24.5 \times 15.5 \times 10.5$ m with a volume of approximately 4000 m^3. The walls consist of 171 groups of three "periacts", i.e., triangular prisms with three surfaces having different reflection properties: absorptive, reflective, and diffusive. Each periact group may be mechanically controlled to choose between six orientations (see Fig. 1). This yields a wide range of possible configurations and resulting acoustic behaviors of the room. The broadband reverberation times vary between 1 and 3 seconds.

In this work, we compare measurements taken in four room configurations, ranging from fully absorptive to fully reflective, with four different source positions and orientations. Spatial analysis methods enable a systematic assessment of the influence of room geometry, boundary conditions, and transducer placement on the anisotropic features of the sound field. We show that the extent of anisotropy depends on the level of absorption at the boundaries, with higher absorption resulting in stronger anisotropy, thus confirming previous results from experiments conducted in reverberant chambers [6], [7]. We also show that diffusive wall conditions reduce anisotropy, which is significant at some frequency bands. Furthermore, changes in source orientation yield varied anisotropy

Corresponding author: *alice.pain@ircam.fr.*

Figure 1: The Espace de Projection, including a detailed view of moving periacts.

patterns on the receiver sphere. This novel finding may be explained by the source directivity, which leads to a differential excitation of the room modes in the rectangular enclosure.
This paper is structured as follows: Section 2 describes the methodology, including the measurement setup and the spatial analysis tools. Section 3 presents the results of the analysis. Section 4 discusses the methodology while Section 5 concludes and lists some remaining open questions.

2. Methodology

This section describes the methods employed for the measurement, treatment, and analysis of the data.

2.1. Measurement setup

Spatial Room Impulse Responses (SRIRs) were captured in a single session in April 2024 using an mh acoustics em64 Eigenmike® Spherical Microphone Array (SMA), supporting 6th-order Ambisonic encoding. The excitation signal was an 11-second logarithmic sine sweep ranging from 20 Hz to 24 kHz at a sample rate of 48 kHz. The SNR was always over 70 dB.
The SMA was placed on a stand 1.70 m above the floor, at the center of the room. Four d&b audiotechnik® E12 loudspeakers were used as sound sources. Their directivity diagrams at 500 Hz, 1 kHz, 2 kHz, and 4 kHz are shown in Fig. 2. They were placed at heights of 1.60 m (sources B, D) and 1.90 m (sources A, C). Source A was pointed at the ceiling with an elevation angle of 90 degrees, while the other sources were kept horizontal. The measurement setup is shown in Fig. 3.

2.2. Periact configurations

Four configurations of Espro's periacts were tested:

- `ABS` : all periacts showing their absorptive side;
- `REV` : all periacts showing their reflective side;
- `DIFF` : all periacts showing their diffusive side;
- `REV-DIFF` : all periacts showing both their reflective and their diffusive side.

The four configurations were uniform over all periacts,

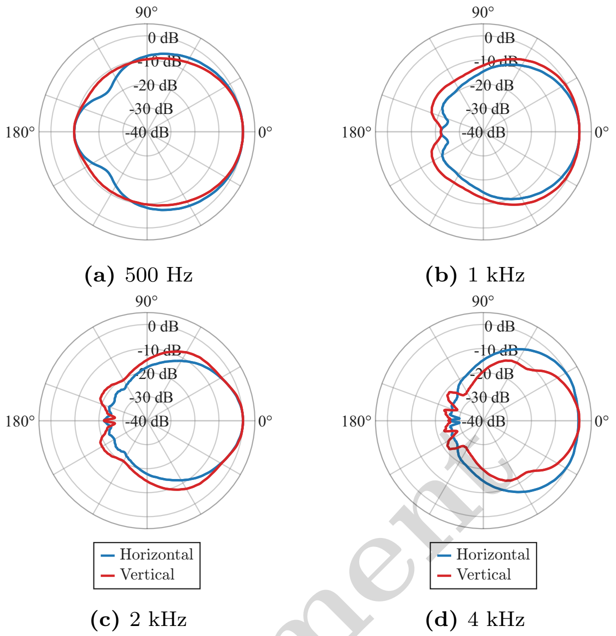

Figure 2: Directivity diagrams of the d&b audiotechnik® E12[1].

except for about twelve periacts that were not mobile, and the lower periacts, which were kept on their absorptive side in all configurations. The resulting reverberation times, estimated via linear regression on the EDC of the omnidirectional Ambisonic component and averaged over the four sources, are given in Table 1, along with the Schroeder frequencies estimated from the broadband reverberation times with the formula:

$$f_{\text{sch}} = 2000\sqrt{\frac{RT_{60}}{V}}, \quad (1)$$

in Hz, where V is the room volume in m^3 and RT_{60} is the 60 dB reverberation time.

Table 1: Omnidirectional reverberation times in seconds estimated for each room condition, averaged over the four sources. The last column gives the estimated Schroeder frequency based on the broadband reverberation times.

Config.	**500 Hz**	**1 kHz**	**2 kHz**	**4 kHz**	f_{sch}
`ABS`	0.91	1.10	1.10	0.83	31.4 Hz
`REV`	2.24	2.49	2.40	1.73	47.1 Hz
`DIFF`	2.20	2.60	2.44	1.71	47.3 Hz
`REV-DIFF`	1.88	2.25	2.14	1.52	44.2 Hz

2.3. Higher-Order Ambisonic encoding, filtering and spatial decomposition

The SRIRs were encoded to 6th-order Ambisonics using the Ambi-X convention, i.e., N3D normalization and ACN channel ordering. The spatial aliasing frequency f_{alias}, i.e., the frequency above which plane waves cannot be resolved spatially, is given by [11]:

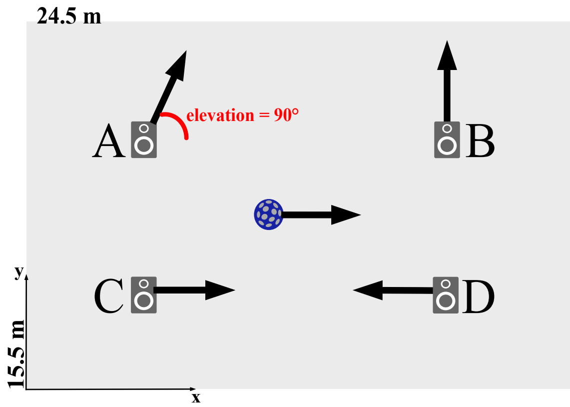

Figure 3: The placement of loudspeakers and the microphone (not to scale). The arrow from the microphone indicates the reference 0-degree direction.

$$f_{\text{alias}} = \frac{cL}{2\pi r}, \tag{2}$$

where c is the speed of sound, L the HOA encoding order and r the radius of the SMA. The em64 has a radius of $r = 4.2$ cm, which yields an aliasing frequency of 7800 Hz assuming $c = 343$ m/s.

At low frequencies, when the wavelengths are comparable to the size of the SMA, the spatial distribution of the sound field cannot be accurately represented. Given these low- and high-frequency limitations, the SRIRs were analyzed using octave-band 2nd-order Butterworth filters with four center frequencies (500 Hz, 1 kHz, 2 kHz, and 4 kHz).

The Ambisonic-encoded SRIRs were further projected onto an equal-area Fliege grid of $D = 196$ steering directions using beamforming to obtain directional RIRs (DRIRs). Given a signal $\mathbf{x}_{\text{SH}}$ encoded at Ambisonic order L, the DRIR $h_d(t) \in \mathbb{R}$ corresponding to direction $\Omega_d = (\phi_d, \theta_d)$ (with $1 \leq d \leq D$) is obtained at each time t via [11]:

$$h_d(t) = \mathbf{Y}_d \, \mathbf{x}_{\text{SH}}(t), \tag{3}$$

where $\mathbf{Y}_d$ is the size $1 \times (L+1)^2$ spherical harmonic encoding vector for look direction Ω_d and $\mathbf{x}_{\text{SH}}(t)$ is the size $(L+1)^2 \times 1$ Ambisonic-encoded signal. This is the maximum-directivity beamformer, which exhibits non-negligible sidelobes.

2.4. Directional analysis

The Energy Decay Curve (EDC), hereafter expressed in dB scale, quantifies the amount of remaining energy at every instant of the decay and is obtained by reverse-integrating the omnidirectional RIR h [12]:

$$\text{EDC}(t) = 10 \log_{10} \left[\int_t^\infty h^2(\tau) d\tau \right]. \tag{4}$$

The Directional EDC (DEDC), first introduced in [13], is obtained for every direction on the spherical grid by performing the same operation on a DRIR h_d:

$$\text{DEDC}(t, \Omega_d) = 10 \log_{10} \left[\int_t^\infty h_d^2(\tau) d\tau \right]. \tag{5}$$

The deviation of each DEDC from the mean DEDC over all directions, or Energy Decay Deviation (EDD), was first introduced in [14] as a way to highlight the direction-dependent features characterizing the decay:

$$\text{EDD}(t, \Omega_d) = \text{DEDC}(t, \Omega_d) - \overline{\text{DEDC}}(t), \tag{6}$$

where

$$\overline{\text{DEDC}}(t) = \frac{1}{D} \sum_{d=1}^{D} \text{DEDC}(t, \Omega_d). \tag{7}$$

3. Results

In this section, the EDD metric is used to characterize the extent of anisotropy during the decay and to display the directional patterns of anisotropy (Section 3.1). Then, reverberation time estimation methods are applied to DEDCs to characterize the spatial dependence of energy decay rates (Section 3.2).

3.1. Directional patterns of incident energy

Modal analysis of sound field decay in rectangular enclosures predicts slower decays for tangential modes than for oblique modes, and even slower decays for axial modes [8], [15]. Thus, during the decay, a concentration of the energy in modes that have slower decay, i.e., axial and tangential modes, is expected. The measurements in Espro show a general trend: energy concentrates in the horizontal axial and tangential modes, particularly the x-axis axial modes (i.e., the receiver's 0-degree azimuth; see Fig. 3 for the coordinate system). The x-axis corresponds to the room's longest dimension, whose axial modes are expected to decay the slowest [16], [17]. In Fig. 4, the EDD of the SRIR measured in the `ABS` condition with source B is projected at four different moments relative to the SRIR's omnidirectional decay (following [13], t_0 is the time of arrival of the direct sound, and $t_{-\text{XdB}}$ is the moment at which the omnidirectional channel of the SRIR has decayed by X dB). The EDDs at t_0 and $t_{-5\text{dB}}$ unsurprisingly display strong anisotropy, showing the direction of arrival of the source and early reflections. However, at $t_{-25\text{dB}}$ and $t_{-35\text{dB}}$, although some mixing has occurred, the sound field remains significantly anisotropic, with energy mostly concentrated on the x-axis. The dominant directions of the energy distribution vary during the decay, which shows that the anisotropy pattern is a property of the room, and not of the position of the source relative to the microphone.

This is further confirmed by Fig. 5, where the EDDs at $t_{-35\text{dB}}$ are plotted for the four different sources in the `ABS` condition. Although all sources show a different orientation relative to the listener, the late decay energy is invariably concentrated along the room's x-axis, and to a lesser extent along the y-axis.

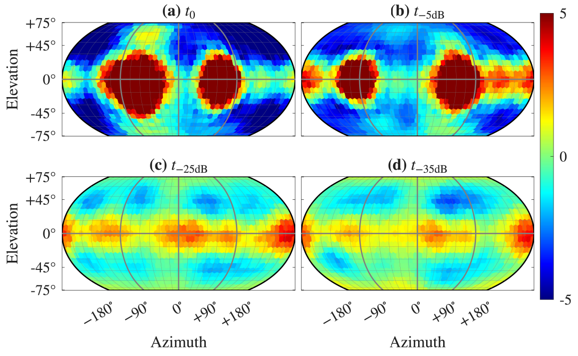

Figure 4: EDDs on the receiver sphere during the decay, in the `ABS` condition, for source B, for the 4 kHz frequency band. The 196-point spherical sampling is visualized using equal-earth projection and a cubic Hermite interpolator. The values are clipped to ± 5 dB.

Influence of source orientation

Despite the mixing process, the anisotropy patterns in the late decay are dependent on the source orientation relative to the room, which impacts the excitation of the axial and tangential modes. Fig. 5 shows the EDDs measured with the four different sources for the `ABS` condition during the late decay. Although there is a general concentration of energy on the horizontal axial and tangential modes, there remain some differences across the sources. A concentration of energy along axial z-axis modes and vertical tangential modes is observed only for source A. This is explained by the fact that source A was pointed at the ceiling. The other sources, aligned with the horizontal plane, did not excite the modes with a vertical propagation direction.

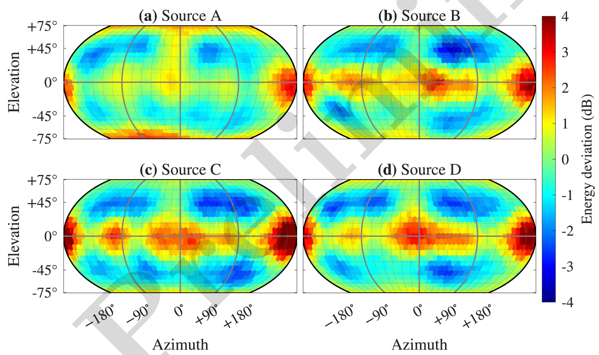

Figure 5: Distribution of incident energy on the receiver sphere at $t_{-35\mathrm{dB}}$, in the `ABS` condition, for the four sources, for the 4 kHz frequency band. The values are clipped to ± 4 dB.

Influence of boundary conditions

As mentioned in the introduction, the boundary conditions have an impact on the strength of the anisotropy effect. These results confirm previous findings in the literature [6], [7], with more absorption resulting in higher anisotropy. Fig. 6 shows that anisotropy is more pronounced for the `ABS` condition than for all the other conditions at t_{-35dB}, with energy deviations from the mean of more than ± 3 dB.

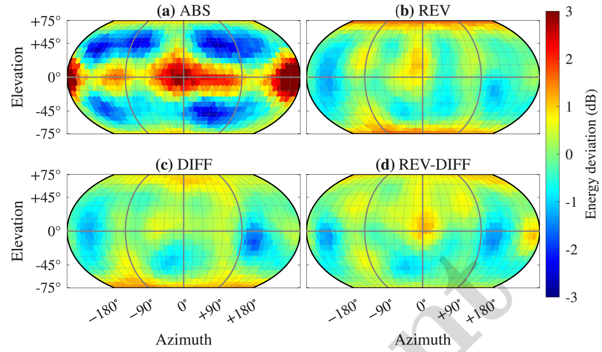

Figure 6: Distribution of incident energy on the receiver sphere at $t_{-35\mathrm{dB}}$, for source D in all conditions, for the 4 kHz frequency band. The values are clipped to ± 3 dB.

In the following, the standard deviation of energy levels over directions is computed in order to quantify the level of anisotropy over time. As shown in Fig. 7, for each source and each room condition, the standard deviation decreases during the early decay until $t_{-20\mathrm{dB}}$. In that early portion, this anisotropy metric shows substantial variations over the four sources. However, after $t_{-20\mathrm{dB}}$, all sources converge to similar values of directional standard deviation, for each room condition. The significantly higher anisotropy of the `ABS` condition is clearly visible at all frequency bands except at 500 Hz. Conditions `REV`, `DIFF`, and `REV-DIFF` show comparable values of anisotropy, except at 4 kHz, where the `REV` condition has a slightly higher anisotropy than the `DIFF` and `REV-DIFF` conditions. Although the omnidirectional decay profiles of these three conditions are very close, diffusion induces an increased isotropy of the incident energy. This is supported by statistical models of late reverberation, which show that diffuse reflections are a sufficient condition for ergodicity [10], [18].

3.2. Directional patterns of reverberation time

The directional decomposition of HOA signals through beamforming allows the estimation of directional reverberation times (DRTs). DRTs are reverberation times estimated with the same methods as omnidirectional reverberation times, applied independently to each DEDC. In this work, linear regression is performed on the exponentially-decaying segment of each DRIR, obtained with instantaneous decay rate analysis for the starting point and noise floor detection for the end point, as detailed in [19]. Here, the DRT differs from the traditional reverberation time definition, which assumes a diffuse field, thus isotropic reverberation and an omnidirectional decay rate.
The range of DRT values for each configuration in the three higher frequency bands is given in Table 2. The variation ranges, significantly higher than the Just

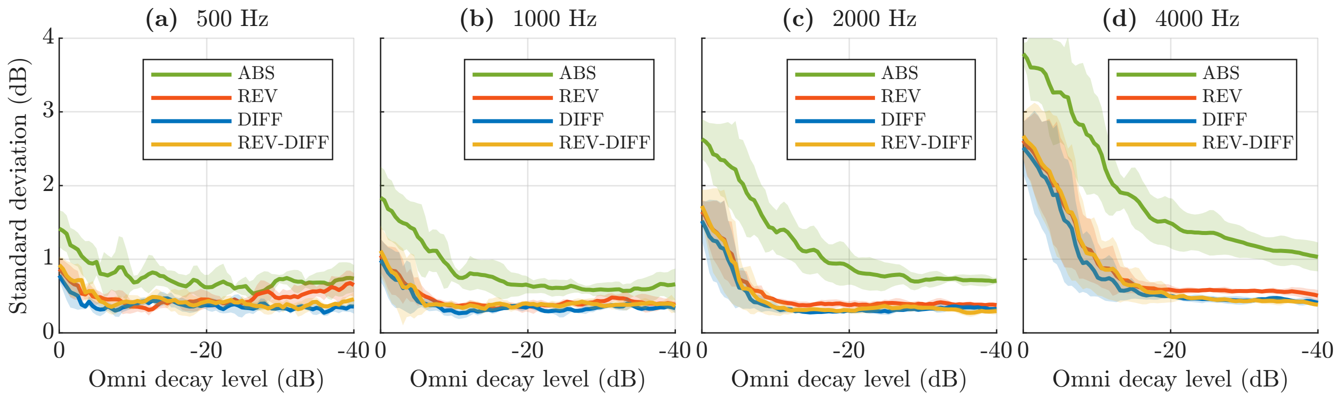

Figure 7: Standard deviation of DEDCs for each room condition averaged over all sources, for each frequency band. The standard deviation over sources is also shown. The values are shown on the relative scale of the omnidirectional energy level corresponding to each DEDC and with a moving average over 20 ms time windows.

Noticeable Difference (JND) of 5% for omnidirectional RT [20], hint at perceivable directional variations, although a JND for DRT remains to be established [5]. Variations increase with frequency and are noticeably larger for the `ABS` condition than for the others.

Table 2: Directional reverberation time variations over all directions for source D.

Config.	1 kHz	2 kHz	4 kHz
`ABS`	1.05–1.18 (13%)	1.00–1.18 (18%)	0.73–0.95 (30%)
`REV`	2.42–2.59 (7%)	2.21–2.42 (9%)	1.45–1.80 (24%)
`DIFF`	2.20–2.29 (5%)	1.94–2.17 (9%)	1.26–1.57 (21%)
`REV-DIFF`	2.54–2.66 (4%)	2.27–2.47 (12%)	1.43–1.72 (25%)

Although the ranges of DRT values are dependent on the room condition, the directional patterns depend more on the source position and orientation than on the room condition. This is shown by Fig. 8, where both the `ABS` and the `REV` conditions show longer DRTs around the x/z vertical plane for source B and around the y/z vertical plane for source D. This is in contrast with the theoretical behavior of the omnidirectional reverberation time, which does not depend on the source position and orientation [12]. When Fig. 6 (top) and Fig. 8 (bottom) are compared, the regions with more energy do not correspond to the regions with longer DRTs (for instance, the x-axis has high EDD values but short DRT values). The mixing of modes with different decay rates is the most likely explanation for the discrepancy between the EDD patterns and the DRT maps: directions showing high energy accumulation (slow-decaying axial modes) do not necessarily show the longest estimated DRTs, since faster-decaying modes may dominate and bias the regression. Thus, the regression results are influenced by the source direction, which favors specific modes.

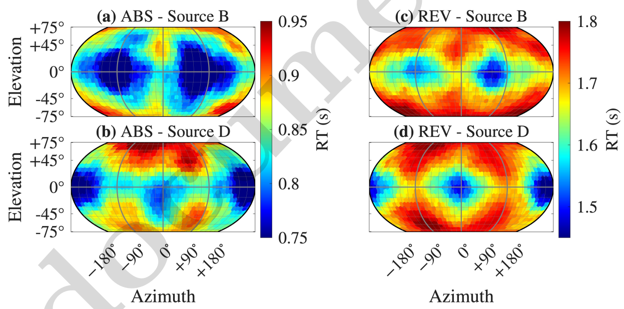

Figure 8: Reverberation times estimated by linear regression for each DRIR on the receiver sphere, for sources B (top) and D (bottom), in the `ABS` (left) and `REV` (right) conditions, for the 4 kHz frequency band.

4. Discussion

The proposed approach has limitations related to both the measurement device and the analysis method. The spatial resolution of the SRIRs is fundamentally limited by the maximum Ambisonic encoding order. At order $L = 6$, the beamwidth of the maximum-directivity beamformer is approximately $180/L = 30°$ [11], meaning that each spatial bin integrates energy arriving from a cone of directions. Each spatial bin may capture contributions from several room modes decaying at different rates. Moreover, the maximum-directivity beamformer used in this work presents non-negligible sidelobes. Energy from directions outside the nominal look direction leaks into each spatial bin, further aggravating the mode mixing. The limited spatial resolution of HOA-encoded signals makes the comparison with theoretical models such as the DRT patterns presented in [9] difficult. In fact, spatial leakage may result in multi-slope decays in individual DRIRs, challenging single-slope reverberation time estimators. Due to this limitation, multi-slope EDC fitting methods should be considered [21], but the interpretation of their results with regard to the spatial smoothing remains to be fully understood.

5. Conclusion

The present work analyzes SRIRs measured in the variable-acoustics shoebox-shaped hall at Ircam using spatial analysis methods to characterize the

anisotropic features of the late reverberation sound field. The hall exhibits noticeably anisotropic late reverberation, with energy concentrating along horizontal axial and tangential modes as predicted by modal theory. The fully absorptive configuration shows the strongest anisotropy, consistent with results from reverberant chambers in the literature [6], [7]. Most notably, the orientation of the source was shown to influence the spatial patterns of anisotropy in the late decay, a result not previously reported in the literature. This is attributed to the selective excitation of room modes by directive sources, which shapes the directional energy distribution beyond the mixing time.
Future work will focus on proposing more accurate directional decay rate estimation methods, accounting for multi-slope decays and for the spatial leakage introduced by beamforming. More measurements are needed to evaluate the influence of non-uniform absorption and diffusive surfaces on anisotropy.

Acknowledgments

This work was funded by a doctoral research grant from the École Normale Supérieure – PSL. The authors would like to thank the members of the EAC team who conducted the measurements, as well as Carlos Agon for interesting discussions on this work.

References

[1] J.-D. Polack, "Playing billiards in the concert hall: The mathematical foundations of geometrical room acoustics," *Appl. Acoust.*, vol. 38, no. 2-4, pp. 235–244, 1993.

[2] J.-M. Jot, L. Cerveau, and O. Warusfel, "Analysis and synthesis of room reverberation based on a statistical time-frequency model," in *Proc. Audio Eng. Soc. 103rd Conv.*, New York, United States, 1997.

[3] M. R. Schroeder, "Statistical Parameters of the Frequency Response Curves of Large Rooms," *J. Audio Eng. Soc.*, vol. 35, no. 5, pp. 299–306, 1987.

[4] B. Alary and A. Politis, "A Dataset for Location- and Direction-Dependent Reverberation Analysis," in *Proc. EAA Forum Acusticum 10th Conv.*, Turin, Italy: European Acoustics Association, 2024, pp. 1663–1670.

[5] B. Alary, P. Massé, S. J. Schlecht, M. Noisternig, and V. Välimäki, "Perceptual analysis of directional late reverberation," *J. Acoust. Soc. Am.*, vol. 149, no. 5, pp. 3189–3199, 2021.

[6] M. Nolan, M. Berzborn, and E. Fernandez-Grande, "Isotropy in decaying reverberant sound fields," *J. Acoust. Soc. Am.*, vol. 148, no. 2, pp. 1077–1088, 2020.

[7] M. Berzborn, M. Nolan, E. Fernandez Grande, and M. Vorländer, "Directional sound field decay analysis in a reverberation room," *J. Acoust. Soc. Am.*, vol. 158, no. 6, pp. 4706–4720, 2025.

[8] F. V. Hunt, L. L. Beranek, and D. Y. Maa, "Analysis of Sound Decay in Rectangular Rooms," *J. Acoust. Soc. Am.*, vol. 11, no. 1, pp. 80–94, 1939.

[9] S. Bilbao and B. Alary, "Directional reverberation time and the image source method for rectangular parallelepipedal rooms," *J. Acoust. Soc. Am.*, vol. 155, no. 2, pp. 1343–1352, 2024.

[10] J.-D. Polack, "Revisiting reverberation," *Acta Acustica*, vol. 9, pp. 30–49, 2025.

[11] B. Rafaely, *Fundamentals of Spherical Array Processing* (Springer Topics in Signal Processing). Cham: Springer International Publishing, 2019, vol. 16.

[12] M. R. Schroeder, "New Method of Measuring Reverberation Time," *J. Acoust. Soc. Am.*, vol. 37, no. 6, pp. 1187–1188, 1965.

[13] M. Berzborn and M. Vorländer, "Investigations on the Directional Energy Decay Curves in Reverberation Rooms," in *Proc. EAA EuroNoise*, Crete, 2018.

[14] B. Alary, P. Masse, V. Valimaki, and M. Noisternig, "Assessing the anisotropic features of spatial impulse responses," in *Proc. EAA Spatial Audio Signal Processing symp.*, Paris, France, 2019.

[15] H. Kuttruff, *Room acoustics*. London, New York: Taylor & Francis, 2006.

[16] P. M. Morse and R. H. Bolt, "Sound Waves in Rooms," *Reviews of Modern Physics*, vol. 16, no. 2, pp. 69–150, 1944.

[17] A. G. Prinn and R. Badeau, "Verification of statistical wave field theory reverberation time predictions," *Appl. Acoust.*, vol. 250, p. 111 337, 2026.

[18] W. B. Joyce, "Exact effect of surface roughness on the reverberation time of a uniformly absorbing spherical enclosure," *J. Acoust. Soc. Am.*, vol. 64, no. 5, 1978.

[19] P. Massé, T. Carpentier, O. Warusfel, and M. Noisternig, "A robust denoising process for spatial room impulse responses with diffuse reverberation tails," *J. Acoust. Soc. Am.*, vol. 147, no. 4, pp. 2250–2260, 2020.

[20] *ISO-3382-1:2009 Acoustics — Measurement of room acoustic parameters*, 2009.

[21] G. Götz, S. J. Schlecht, and V. Pulkki, "Common-Slope Modeling of Late Reverberation," *IEEE/ACM Transactions on Audio, Speech, and Language Processing*, vol. 31, pp. 3945–3957, 2023.